Site-Controlled Single-Photon Emitters Fabricated by Near-Field Illumination

Site-controlled single photon emitters fabricated by near field illumination

F. Biccari,[1, a)] A. Boschetti,[1] G. Pettinari,[2] F. La China,[1] M. Gurioli,[1] F. Intonti,[1] A. Vinattieri,[1] M. S. Sharma,[3] M. Capizzi,[3] A. Gerardino,[2] L. Businaro,[2] M. Hopkinson,[4] A. Polimeni,[3] and M. Felici[3]

[1)]*Dept. of Physics and Astronomy, and LENS, University of Florence, Via Sansone 1, I–50019 Sesto Fiorentino (FI), Italy*

[2)]*Istituto di Fotonica e Nanotecnologie (IFN-CNR), Consiglio Nazionale delle Ricerche, Via Cineto Romano 42, I-00156 Roma, Italy*

[3)]*Dept. of Physics and CNISM, Sapienza - University of Rome, Piazzale Aldo Moro 5, I-00185 Roma, Italy*

[4)]*Dept. of Electronic and Electrical Engineering, University of Sheffield, Sheffield S3 3JD, United Kingdom.*

(Dated: 20 September 2017)

A thoroughly revised version of this paper was published on Advanced Materials (Wiley): doi: 10.1002/adma.201705450

Many of the most advanced applications of semiconductor quantum dots (QDs) in quantum information technology require a fine control of the QDs' position and confinement potential, which cannot be achieved with conventional growth techniques. In this work, a novel and versatile approach for the fabrication of site-controlled QDs is presented. Hydrogen incorporation in GaAsN results in the formation of N-2H and N-2H-H complexes, which neutralize all the effects of N on GaAs, including the N-induced large reduction of the band-gap energy. Starting from a fully hydrogenated GaAs/GaAsN:H/GaAs quantum well, the N-H bonds located within the light spot generated by a Scanning Near-field Optical Microscope tip were broken, thus obtaining site-controlled GaAsN QDs surrounded by a barrier of GaAsN:H (laterally) and GaAs (above and below). By adjusting the laser power density and exposure time, the optical properties of the QDs can be finely controlled and optimized, tuning the quantum confinement energy over more than 100 meV and resulting in the observation of single photon emission from both the exciton and biexciton recombinations. This novel fabrication technique reached a position accuracy of 50 nm and it can be easily applied to the realization of more complex nanostructures.

Keywords: Site-controlled quantum dots, single-photon emission, dilute nitrides, laser writing

[a)]Corresponding author: francesco.biccari@unifi.it

Semiconductor quantum dots (QDs) have attracted increasing interest in the last decades. Thanks to their tunable emission energy and to their narrow luminescence linewidth, they may find – and, in some instances, already have found – possible applications in many fields[1,2], from light-emitting devices (e.g. LED and lasers) to biology, from photovoltaics to sensor devices. In addition, owing to their ability to act as sources of non-classical light states, QDs might serve as the main building blocks of several potentially ground-breaking devices, enabling the first practical implementation of quantum information technology (e.g., quantum computation, quantum teleportation, quantum cryptography)[3]. In particular, epitaxially grown semiconductor QDs, as opposed to other quantum emitters such as single atoms or colloidal QDs, present the advantage of being natively embedded within a solid-state matrix, which fixes their position and makes them uniquely suited for the integration in electronic devices.[4]

Coupling QDs with photonic structures, and particularly with photonic crystal (PhC) microcavities[4,5], is a fundamental step towards the practical implementation of quantum devices. Indeed, such a coupling can increase the radiative recombination rate of the QD[4,5], thus increasing the speed and brightness of the device and reducing the negative effects of dephasing[6,7], thereby greatly improving the performance of QDs as sources of entangled photons[4,5]. It can also help to couple light into waveguides, with the goal of realizing all-integrated optical chips. The stochastic coupling of self-assembled QDs to photonic crystal cavities has been demonstrated both in the weak[8] and strong coupling regimes[9,10]. On the other hand, for years, the strategy to deterministically align a photonic crystal cavity to a single QD was simply based on the fabrication of the cavity after the QD was first located by microscopy techniques[11].

However, these approaches are not easily transferable to the fabrication of devices with the ability to go beyond the proof-of-concept stage. A precondition for the fabrication of integrated complex devices and their mass production is indeed the availability of a scalable, deterministic technology for the fabrication of QDs that are spatially ordered, uniformly sized, and spectrally matched with respect to the device architecture. This challenge cannot be met using conventional, bottom-up growth techniques, which, however, currently give the best results in terms of the optical properties of the resulting QDs. In particular, the main drawback of the most widely used standard growth methods (i.e., Stranski-Krastanow and Droplet Epitaxy) can be identified with their lack of control over the lateral position of each QD.[4] As a reference, we can consider that in PhC cavities the typical spatial full width at half maximum (FWHM) for the field at the antinode is slightly smaller than the lattice constant of the PhC, which in turn is about 0.25λ, where λ is the wavelength

in vacuum of the considered cavity mode. For typical systems operating at visible/NIR frequencies, this means a spatial extension of about 200 nm.[5] Therefore, the integration of a quantum emitter with a PhC cavity will realistically require a spatial positioning accuracy better than 50 nm. As it regards the required spectral matching between the QD and the cavity mode, giving an absolute numeric threshold might be significantly more difficult, considering that the coupling depends on several factors such as the quality factor (Q) of the mode and the QD-PhC cavity coupling strength (g). However, the general consensus seems to indicate that a control of 1-2 meV at least, based on typical QD-PhC systems, would be a reasonable requirement for the emission energy of the QD.[5]

In the last two decades, several methods have been developed to control the QD nucleation position[4]. Perhaps the most successful approach is represented by the self-limited growth of QDs into inverted pyramidal holes etched in a GaAs substrate[12,13]. This approach gave a record-low inhomogeneous emission broadening of 1.4 meV[14], and it was used for the integration of site-controlled QDs with PhC cavities, showing weak coupling[15–18]. QDs grown in larger pyramids (with typical size of 7.5 µm), not integrable in PhC cavities, have reached a very good homogeneous broadening of 10 µeV[19]. The weak-coupling regime was recently achieved in other integrated QD-PhC cavity systems, based on position-controlled QDs obtained by providing preferential sites for the nucleation of self-assembled dots. Such nucleation sites can be defined, for example, by growing InP pyramids by selective-area epitaxy[20–22], or by patterning the substrate with nano-hole arrays[23–26]. The main characteristics of these site-controlled QD fabrication techniques are reported in Table 1. For the sake of completeness, we mention that up to now strong coupling was not yet observed in site-controlled QDs coupled with photonic cavities, to the best of our knowledge. Other approaches to the fabrication of site-controlled QDs, for which the integration with PhC cavities is still to be demonstrated, include the self-organization of individual InAs QDs by scanning tunneling probe-assisted nanolithography[27]; the "vicinal substrate" approach[28]; the nucleation of InAs QDs on strain modulated buffer layers grown on submicron mesa array[29]; and quantum well etching[30]. As we stated before, the optical properties of site-controlled QDs do not reach the quality of self-assembled ones. However, it should be mentioned that the Purcell effect and resonant excitation[4] can be employed to enhance the effective quantum efficiency and to reduce the effects of linewidth broadening, respectively.

Even though in principle all these nanofabrication methods are scalable, they all rely on complex lithographic procedures, followed by often cumbersome processing steps in a clean room environment, such as wet or dry etching. In this work, we present a new method to fabricate site-controlled,

Table 1. List of site-controlled QD fabrication techniques with their main properties: type of QDs, position accuracy Δx, inhomogeneous broadening ΔE, use of lithographic and etching processes.

Technique	Type of QDs	Δx (nm)	ΔE (meV)	Lith.+etch.
Pyramids[21,22]	InAs/InP	50	50	yes
Inv. Pyr.[14,15]	InGaAs/GaAs	<50	1.4	yes
Nanoholes[24,25]	InAs/GaAs	80	70	yes
Masks+H[31,32]	GaAsN/GaAs	20	30	yes
This work	GaAsN/GaAs	50	20	no

single-photon emitting QDs based on the effects of hydrogen on the properties of GaAsN (or other dilute nitrides[33,34], such as GaPN and InGaAsN) without the need for lithographic techniques or a particularly controlled environment. As we will discuss in the following, this method combines short fabrication times (about 1 s per QD) with high positioning accuracy (about 50 nm), in principle allowing both for the realization of large, ordered QD arrays and for the precise placement of individual QDs in the desired points of a photonic structure.

Dilute nitrides are a class of III-V semiconductor alloys, where N is present in a small percentage (typically less than 4-5%) in the V sub-lattice[34]. The most representative material among them is $GaAs_{1-x}N_x$. Other derived materials, like InGaAsN and InGaAsNSb, are very popular in multijunction solar cells[35] and telecommunication devices, mainly because their band gap value can be tailored to match the wavelengths that optimize the performance of such devices (e.g., $\lambda = 1.31$-$1.55\,\mu$m for telecommunications)[33,36]. Recently, the possible use of dilute nitrides in spintronics has also been proposed[37]. Indeed, the introduction of nitrogen in GaAs, and in other III-V semiconductors, strongly perturbs the conduction band structure, giving rise, among other effects, to a large, tunable reduction of the band gap[38,39] and to the modification of the electron g-factor[40]. For instance, the band gap of $GaAs_{0.989}N_{0.011}$ is about 1.29 eV at 10 K, about 230 meV lower than the GaAs band gap value[41,42], while the electron g-factor rises to a value of about 1 (being -0.44 in GaAs) already for a nitrogen concentration of 0.1%[40].

Another striking property of dilute nitrides is the effect that hydrogen has on them[33]. Indeed, H

atoms form stable N-2H and N-2H-H complexes[33,43–45] that wipe out the effects of nitrogen, thus gradually restoring the band gap[46–48], effective mass[49], spin properties[40], refractive index[50], lattice constant[45,46,51], and ordering[52] of the N-free materials. By introducing hydrogen in a controlled manner, all these properties can be finely tuned; moreover, by allowing H incorporation only in selected regions of the sample, it is possible to achieve a spatially tailored modulation of the band gap energy[53], as well as of the lattice constant[54], in the growth plane. In particular, depositing H-opaque masks on the surface of a GaAs/GaAsN/GaAs quantum well before H irradiation allows for the realization of site-controlled nanostructures with arbitrary shape and size, like QDs[31,55] or wires[56]. This technique allowed also to achieve the weak-coupling regime in a QD-PhC cavity system[32,57]. In Table 1 the main characteristics of this fabrication technique are reported. While this post-growth method for the fabrication of site-controlled nanostructures presents significant advantages over the techniques described earlier, even in this case, nanolithography techniques and etching steps are needed for the nanopatterning of the surface.

In the present work, on the other hand, we exploit the possibility to break N-H bonds by illuminating the sample with a laser light of proper wavelength[58,59]. In particular, we are able to achieve a high spatial control of the hydrogen removal process by focusing the laser light with the dielectric tip of a Scanning Near-field Optical Microscope (SNOM), which allows us to overcome the diffraction limit of objective lenses[60], thus obtaining site-controlled GaAsN QDs. Before proceeding any further, it is worth noting here that this fabrication process was performed at room temperature and in air, without any particular treatment of the sample's surface.

The sample used in this work is a fully hydrogenated GaAs/GaAsN:H/GaAs quantum well (QW). In order to test the H removal process in a condition similar to that needed for its realization in a photonic crystal cavity, the QD fabrication was performed on an array of well-separated circular areas where the QW is suspended with respect to the substrate, as shown in Figure 1a and 1b. The QD fabrication was performed by exposing for a few seconds a nanometric region of the membrane surface, ideally the central region, with the 514.5 nm line of a continuous wave (CW) argon laser by means of a SNOM setup in illumination mode, equipped with a dielectric tip. Exploiting the optical near field of the tip, we aim to remove hydrogen[58,59] from the GaAsN:H layer of the QW in an area smaller than the typical spot size (about 500 nm) obtained at this wavelength with a high NA objective lens. A sketch of the QD fabrication process is reported in Figure 1c. The excitation power and exposure time are varied to optimize the fabrication process. Details on the sample preparation and QD characterization techniques are reported in the Experimental Section.

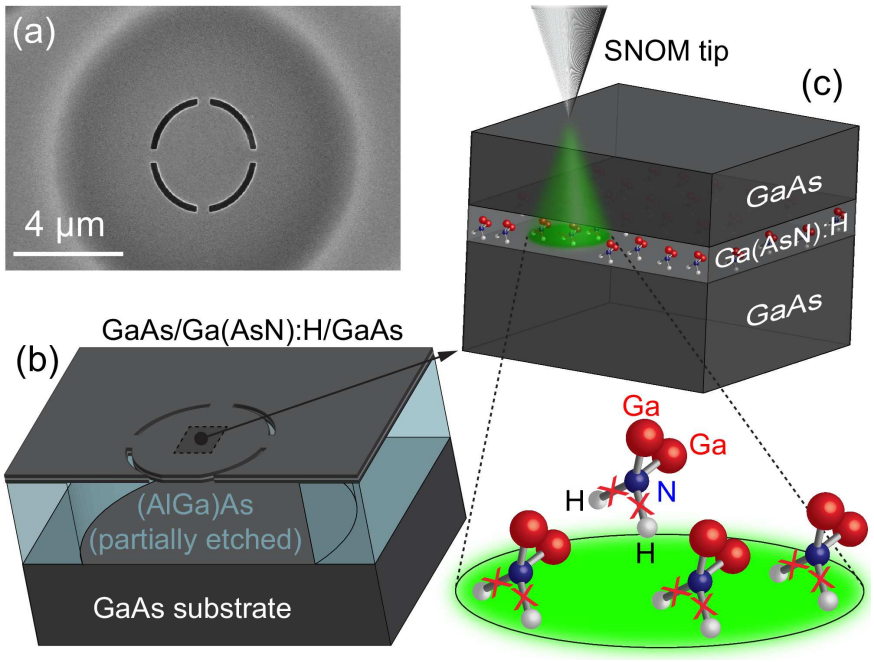

Figure 1. Sample description and sketch of the QD fabrication technique. (a) Top view by SEM of a suspended quantum well structure (membrane) within which the QDs are fabricated. The black areas are the apertures opened in the membrane layer by Reactive Ion Etching to let HF penetrate below the QW and etch the sacrificial AlGaAs layer away. In the figure, the circular region from which the sacrificial layer has been removed is visible as a dark-gray area underneath the released membrane. (b) Sketch of the suspended membrane sample. (c) Illustration of the QD fabrication process: a SNOM tip coupled with a laser beam generates a near-field hot spot, within which the N-H bonds of the GaAsN:H layer are broken, leaving a GaAsN QD.

In Figure 2a we have reported the PL spectra of five representative GaAsN QDs fabricated at different powers, from 1.1 mW to 0.7 mW, and with the same exposure time (1 s). The PL spectrum of the GaAs/GaAsN/GaAs QW before hydrogenation is also reported for comparison reasons, as the QW emission energy (about 1.30 eV in our case) represents the lower limit for that of the QD. Indeed, when hydrogen is removed from an area large enough that the H-induced confinement effects are negligible, the fabricated QDs approach the QW's behavior. This situation can be attained for either high fabrication powers or long exposure times. By keeping the exposure time fixed while reducing the fabrication power, indeed, the QD diameter is expected to decrease. In turn, this should result in a larger confinement-induced blueshift, which can be observed rather clearly in the micro-PL spectra displayed in Figure 2a.

The behavior described above is summarized in Figure 2b, wherein the average PL emission energy is plotted versus the fabrication power for two different set of QDs: one fabricated with 1 s exposure time (blue dots) and the other one with 5 s (red squares). Two colored bands are also plotted as a guide for the eye: they have a width of 20 meV, corresponding to the inhomogeneous broadening of the emission energy of the QDs. As expected, the QD emission energy decreases, i.e., the dot size increases, also by increasing the exposure time. As noted above, for high excitation powers the observed trends both seem to saturate at the value of the QW energy, corresponding to negligible H-induced confinement effects. When the excitation power tends to zero, on the other hand, the two datasets tend to rather different asymptotic QD energies, i.e., QD sizes. This observation seems to suggest a non-trivial dependence on the excitation conditions for the effective size of the "hot spot" generated by the photons impinging on the sample. This is perhaps not surprising, given that the size of the hot spot is determined by the combined role of several complex phenomena, among which photon absorption and heat dissipation, simultaneously taking place inside the material. While it is beyond the scope of this work to provide an accurate theoretical modeling of the dependence of the QD size on the excitation conditions, its full characterization is crucial to maximize our control over this novel nanofabrication technique. Figure 2b provides a clear example of the importance of the excitation conditions, as the range of energy tunability attainable for the fabricated QDs nearly doubles –going from 70 meV to 130 meV– as the exposure time is decreased from 5 s to 1 s.

In Figure 2c we reported the PL intensity map of the 1.315 eV emission peak of a QD fabricated with a laser power of 1.1 mW for 1 s (spectrum in Figure 2a), superimposed to a SEM image of the same area. The alignment was done analyzing the intensity of the background signal coming from the substrate. Indeed, due to the different refractive index contrast between released and non-released areas, this signal is greatly reduced in the released areas, thus allowing us to clearly define the extension of the suspended membrane. The emission in Figure 2c comes from the center of the membrane and its spatial FWHM is about 1 μm, which is equal to the spatial resolution of the setup, as expected.

We have also used the SNOM setup to measure the sample topography, thus testing the surface of the membrane for possible morphological modifications after QD fabrication. For 1 s exposure time, as long as the fabrication power is less than 1.2 mW, no damage of the surface is observed, as shown in the topographic map of Figure 2d. When the power is 1.2 mW or more, on the other hand, a little dip is created in the exposed region, as shown in the topography of Figure 2e, and in the

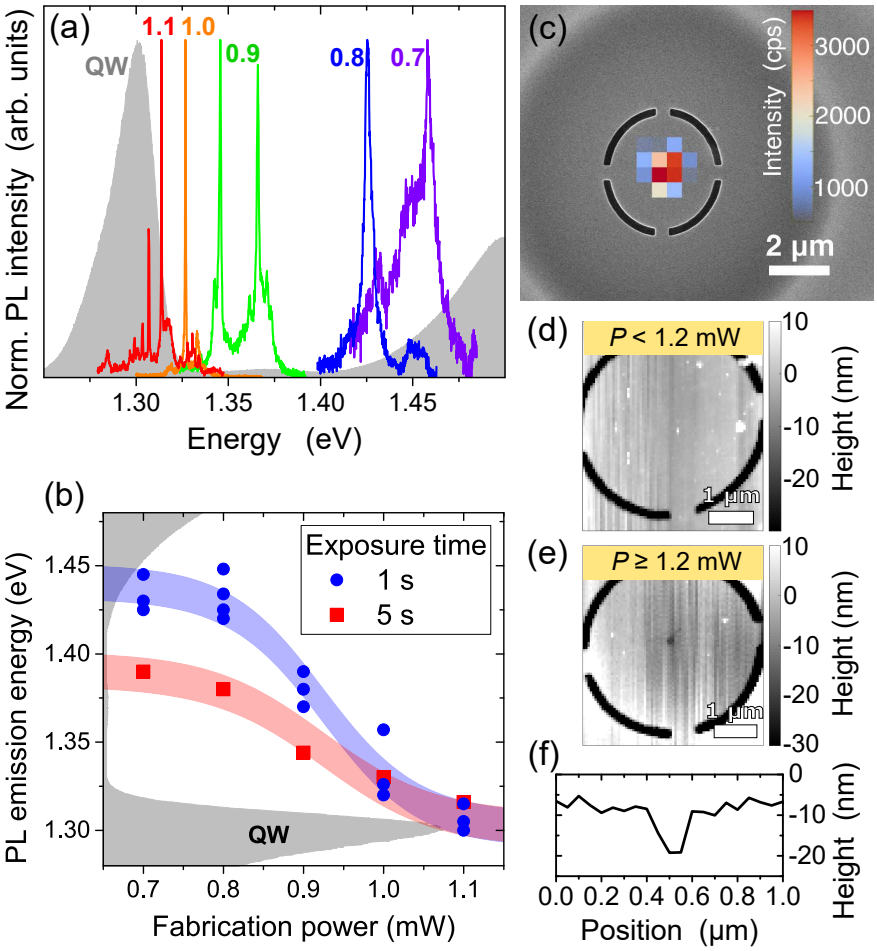

Figure 2. (a) PL spectra at 10 K of five GaAsN QDs fabricated at different powers, distinguished by colors, and with the same exposure time (1 s) superimposed to the PL spectrum of the GaAs/GaAsN/GaAs QW before hydrogenation (gray areas). The fabrication powers, in unit of mW, are provided as labels. (b) PL emission energy at 10 K of several GaAsN QDs as a function of the fabrication power. Blue dots and red squares represent 1 s and 5 s exposure time, respectively. The colored bands are a guide for the eye. (c) PL intensity map at 10 K of the emission peak at 1.315 eV of one of the GaAsN QDs shown in (a), fabricated at 1.1 mW for 1 s. The emission has a round shape and a spatial FWHM of 1 µm, equals to the setup resolution. (d) Topography map of the membrane surface after the fabrication of a QD (fabrication power of 1.1 mW). Using 1.1 mW or less, no damage of the surface is observed. (e) Topography map of the membrane surface after the fabrication of a QD with a fabrication power of 1.2 mW for 1 s. Using 1.2 mW or more, a clear damage of the surface is observed. (f) Depth profile of the membrane pit shown in (e).

relative depth profile of Figure 2f. The measured depth of the dip is about 10 nm, while its FWHM is about 100 nm. This dip represents an upper limit for the possible dimensions of the fabricated QDs, which are actually expected to be much less than 100 nm, at least for the fabrication powers giving rise to sizable confinement effects.

Using the emission energies in Figure 1b we can estimate the size of our QDs (see Supporting Information for details). We assume that they have a cylindrical shape, with a radius R, determined by the QD fabrication parameters, and thickness $L = 6$ nm, the same of the original QW, since it is reasonable to assume that hydrogen is fully removed from the entire thickness of the GaAs/GaAsN/GaAs QW. We obtain $2R = 4.8$, 5.0, 6.1, 9.2, 13 nm for the QDs created with 0.7, 0.8, 0.9, 1.0 and 1.1 mW fabrication power (1 s time exposure), respectively. The error on $2R$ is about $\pm 15\%$. This proves that with the SNOM tip we have removed hydrogen from an area much smaller than the diffraction limit.

These dimensions are surprisingly smaller than the beam size. Indeed, as we stated previously, the beam size of the tip in the GaAsN:H layer is expected to be about 200 nm. In order to form a QD, the removed hydrogen should, in principle, diffuse out of the central region and this can take place only if a temperature gradient is present. This feature can explain why we can obtain smaller QDs with respect to the width of the fabrication beam: while the wavelength and excitation power determine the amount of broken N-H bonds, the temperature gradient and the exposure time determine the H diffusion and therefore the diameter of the QD. This conclusion is supported by the fact that, at low temperature (10 K) or in the case of a non-patterned sample, the excitation power must be increased to obtain QDs similar to those fabricated at room temperature and/or on the suspended membranes. Even though no measurement of the QD position distribution with respect to the center of the tip is available, we can reasonably think that the QD is formed under the center of the tip, in a spot which can be pessimistically considered as half of the end diameter of the tip, giving, in our case, about 50 nm[61,62]. This number gives the ultimate limit of the spatial precision of our fabrication technique, since other effects like tip positioning and tip quality can increase this limit. As previously stated, this limit is similar to that established for other site-controlled QD fabrication techniques (see Table 1), and it satisfies the requirements for the controlled integration of a QD with photonic crystal cavities.

From the data reported in Figure 2b, an emission inhomogeneous broadening of about 20 meV can be inferred for the QDs fabricated with a 1 s exposure time. The two guides for the eyes in Figure 2b have this width. It is worth noting that the lower limit of the inhomogeneous broadening

of the QDs fabricated with this technique is roughly given by the broadening of the starting QW, which is mainly due to roughness at the GaAsN/GaAs interfaces and to nitrogen random fluctuations in GaAsN. Since in the present case, the inhomogeneous broadening of our QDs is similar or even smaller than the QW broadening, we can only conclude that the spectral reproducibility of our QD fabrication technique gives rise to a broadening much smaller than 20 meV. As discussed above (see Table 1), other site-controlled QD fabrication techniques show larger QD inhomogeneous broadenings, except for the technique based on inverted pyramids. Even though the spectral accuracy of our technique does not satisfy the requirements for a controllable integration of QDs in PhC cavities, we have to mention that it does not give rise to any appreciable additional broadening with respect to the QW broadening. This means that we could reach much smaller QD inhomogeneous broadening simply by employing higher-quality QWs.

In some cases, our QDs show several peaks (see, e.g., Figure 3a), which can be identified by studying their PL emission intensities as a function of the excitation power. Figure3a shows three PL spectra of the same QD acquired for different excitation powers. All the displayed spectra are characterized by the presence of two peaks, with a clearly different dependence of the PL intensity on the excitation power, as summarized in Figure 3b. According to a Poissonian model for the level occupation probability[63], the exciton (X) and bi-exciton (XX) PL line intensities, I_{PL}, follow different filling dynamics, as described by the expression

$$I_{\mathrm{PL}} = C(\alpha P^{\beta})^{n} \exp(\alpha P^{\beta}) \ , \tag{1}$$

where $n = 1$ for X and $n = 2$ for XX, P is the excitation power, and C, α, and β are three constants. The term αP^{β} corresponds to the average number of excitons present in the QD, $\langle n \rangle$, for a given excitation power. Fitting the experimental data with Equation (1), we obtain that the peak at 1.325 eV can be attributed to the X recombination, while the peak at 1.315 eV to the XX recombination. The fitting parameters result to be $\alpha = (1.01 \pm 0.14)\,\mu\mathrm{W}^{-\beta}$ and $\beta = (1.14 \pm 0.06)$ for the QD under consideration. The line broadening and the relative spectral position confirm our attribution. It is known that the most important contribution to the spectral broadening are the electric field fluctuations generated by charged defects around the QD. The relative position of the charged defects results in a different quantum confined Stark shift amplitude for each excitonic complex. It turns out that X is nearly always broader than XX[64], as we also found in our case. Moreover, XXs have usually a negative binding energy[65], therefore their luminescence should be observed at lower energies with respect to the exciton, as also observed in our case.

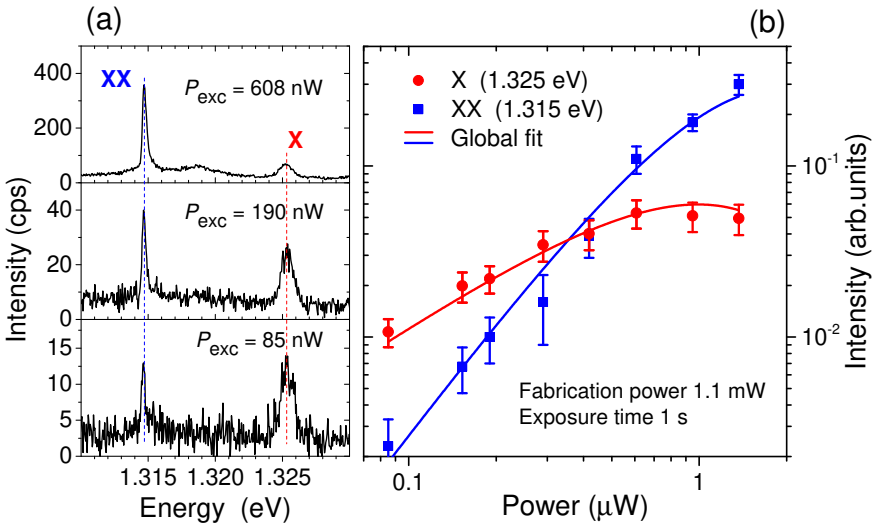

Figure 3. Analysis of the PL ($T = 10$ K) as a function of the excitation power for a GaAsN QD fabricated at 1.1 mW with an exposure time of 1 s. (a) Three PL spectra of the QD, acquired at different excitation powers. Two peaks are present, characterized by a different power dependence. At 190 nW, the FWHMs of the two emissions at 1.325 eV (X) and 1.315 eV (XX) are 300 μeV and 900 μeV, respectively. (b) Intensity versus excitation power for the two peaks shown in (a). The continuous lines are fits of the data with Equation (1), which allow us to identify the two peaks with the exciton (X, 1.325 eV) and biexciton (XX, 1.315 eV) emissions. This identification is consistent with the relative values of the FWHMs.

As a last remark, the X line reported in Figure 3b shows a saturation power of about $P_{\rm sat} \approx 1.1$ μW. The saturation power of X (i.e., the value of P for the maximum occupation probability) allows us to estimate the capture volume V of the QD[63]. Since at saturation the average number of excitons in a QD is 1, $\langle n \rangle = 1$, we can write $VG\tau = \langle n \rangle = 1$, where G is the e-h pair generation term and $\tau \approx 1$ ns is the lifetime of the e-h pairs. Considering the GaAs absorption coefficient[66] at 532 nm, $\alpha = 7 \times 10^4$ cm^{-1}, and an average generation term given by $G = \alpha P_{\rm sat}/(AE_{\rm ph})$, where $A = 1$ μm^2 is the spot area and $E_{\rm ph}$ the 532 nm photon energy, we can estimate a capture volume of about 4.9×10^4 nm^3. Assuming a cylindrical geometry of the QD with an height $h = 6$ nm (the entire height of the QW) and radius $R \approx 11$ nm as calculated above, we can estimate the capture length ($L_{\rm c}$) of the QD, considered constant all around the nanostructure. We obtain about $L_{\rm c} = 17$ nm, much larger than the QD size, indicating the fairly good quality of the material.

We have then measured the normalized second order autocorrelation function, $g^{(2)}(\tau)$, to test the single-photon emitter nature of the realized QDs. In Figure 4a we have reported the spectrum of the QD of Figure 3, fabricated at 1.1 mW with 1 s exposure time (red line), which shows X and XX

emission lines. In Figure 4b the $g^{(2)}(\tau)$ measured on the XX emission line of this QD is shown. Analogously, in Figure 4a we have reported the spectra of two additional QDs: one fabricated with a power of 1.0 mW and a 1 s exposure time while for the other we employed at 7 mW for 1 s, using a different optical fiber. In Figure 4c and 4d the $g^{(2)}(\tau)$ of their observed X emission lines are reported.

All the $g^{(2)}(\tau)$ in Figure 4 were fitted with curves (reported as solid black lines) based on the solutions of a system of rate equations, developed by taking into account the main processes leading to the capture, relaxation, and recombination of carriers in and out of the QD (for a full description of the model, see Ref. 57). For the QDs reported in Figure 4b and 4c the fit yields a carrier capture time, τ_{cap}, of 0.27 ns and 0.14 ns, respectively, while the exciton recombination time is $\tau_{\text{rad}} \sim 1$ ns for both QDs. The black curve reported in Figure 4c is actually not a fit, as we fixed $\tau_{\text{rad}} = 1$ ns and $\tau_{\text{cap}} = 0.2$ ns, while also including a classically correlated background that accounts for 50% of the coincidences (a strong background is clearly visible in the PL spectrum shown in Figure 4a; the $g^{(2)}$ of the sole QD is displayed in Figure 4d as an orange line, renormalized to the maximum of the lateral peaks).

The obtained values of the $g^{(2)}(\tau)$ at zero delay ($\tau = 0$) for the emissions reported in Figure 4b-d are 0.25, 0.06, and 0.10, respectively. These values, lower than 0.5, prove that our emitters are single photon sources. The $g^{(2)}(0)$ does not show a zero value because, in order to shorten the time measurement, the power was increased, leading to a larger probability of the QD ground state re-population from higher energy levels and to spurious emission from the substrate.

It is worth noting the large FWHM (≈ 2 meV) of the QD indicated with label (d) in Figure 4a. Throughout our experiments, we systematically found that smaller QD dimensions corresponded to larger spectral broadening and to lower QD efficiencies. For the smaller QDs, i.e., for low fabrication powers, the low efficiency prevented us from measuring the $g^{(2)}(\tau)$ without resorting to prohibitively long acquisition times. Both the low efficiency and the larger line broadening are consistent with an increased effect of the environment (e.g., non-radiative defects, fluctuating charges) on the properties of smaller QDs. On the one hand, this might point to an increased role of the surface (in our case, of the QW interfaces, where defects and extra charges are known to concentrate) as the QD size decreases. On the other hand, it is not surprising to observe this behavior in shallower, less confined QDs, characterized by significantly more delocalized exciton wavefunctions.

In conclusion, we have demonstrated the possibility to fabricate site-controlled QDs exploiting

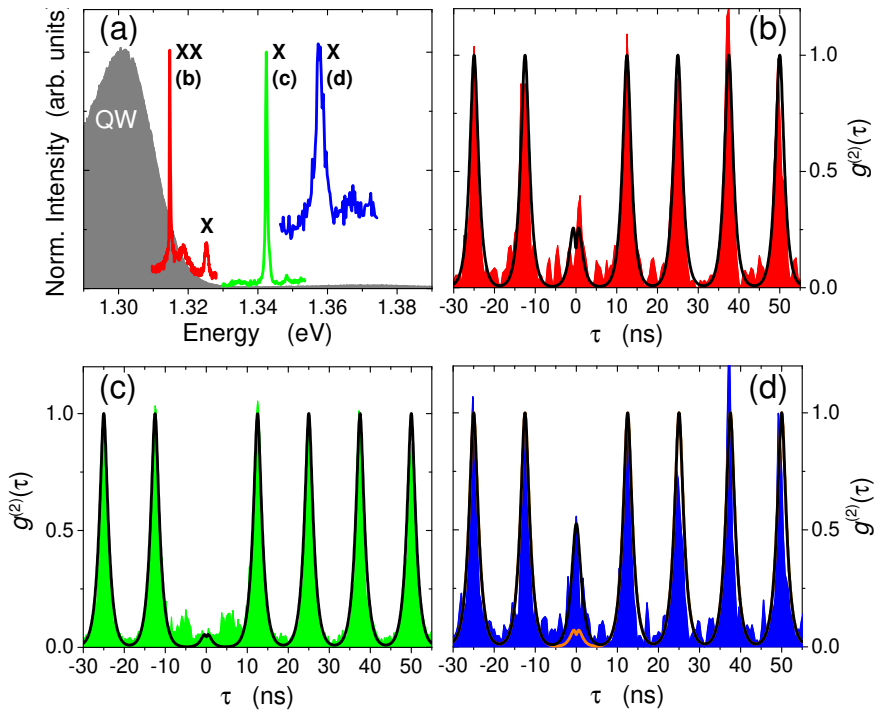

Figure 4. (a) PL spectra at 10 K of three GaAsN QDs emitting at different energies, distinguished by colors, superimposed to the PL spectrum of the GaAs/GaAsN/GaAs QW before hydrogenation (gray area). The labels X and XX indicate the exciton and bi-exciton emissions, respectively. The labels (b), (c), and (d) indicate in which panel is reported the corresponding normalized second order autocorrelation function, $g^{(2)}(\tau)$. The value of $g^{(2)}(0) < 0.5$ is a proof of the single photon emitter nature of the GaAsN QDs fabricated with our technique. The dot (b) was fabricated with 1.1 mW for 1 s, the dot (c) with 7 mW for 1 s using a different optical fiber and the dot (d) with 1.0 mW for 1 s. Solid black lines in (b), (c), (d) represent the fit of the $g^{(2)}(\tau)$ with a QD microstate model explained in the text and detailed in Ref. 57. Since the fit in (d) was obtained considering also a classical correlated background, the contribution of the sole QD (renormalized to the maximum of the adjacent peaks) is reported as a solid orange line.

the optical near field of a tapered dielectric fiber (SNOM tip) and the effects of hydrogen on the properties of GaAsN. This fabrication technique showed a spatial accuracy of the order of 50 nm and an inhomogeneous broadening of about 20 meV. While the spatial accuracy is sufficient for the deterministic integration of a site-controlled QD with a PhC cavity, the inhomogeneous broadening obtained for our QDs is too large. However such broadening is due entirely to the linewidth of the GaAsN QW we employed, suggesting a negligible broadening due to our fabrication technique. Some QDs have shown the presence of both biexciton and exciton emissions, an important feature

for the possible employment of these QDs as sources of entangled photon pairs[4].

It is worth noting that the QD fabrication was performed in air, at room temperature, and without any particular lithography or etching procedure. Further, this fabrication technique has several other advantages: 1. absence of a wetting layer[4]; 2. possibility to cover both telecommunication wavelength windows by tuning the nitrogen concentration and/or introducing indium in GaAsN[33]; 3. very broad range of applications, since in principle this technique can be used to directly write, not only QDs, but any complex planar nanostructure, such as quantum wires, quantum rings, or QD molecules/chains; 4. *rewritability* of the sample. A hydrogen irradiation can "erase" the nanostructure, making the sample ready for another nanostructure writing; 5. possibility to tune, not only the band gap, but also the refractive index of the material, thus allowing for the realization of rewritable waveguides[50]. In conclusion, this novel fabrication technique paves the way to the easy integration of QDs in arbitrary photonic structures with a controllable top-down approach.

EXPERIMENTAL SECTION

Sample preparation. We prepared a fully hydrogenated GaAs/GaAsN/GaAs quantum well (QW), grown by Molecular Beam Epitaxy with the following structure: a GaAs buffer (130 nm) is deposited on a (001) GaAs substrate, followed by an $Al_{0.7}Ga_{0.3}As$ sacrificial layer (1500 nm), a GaAs lower cladding (130 nm), a $GaAs_{0.989}N_{0.011}$ layer (6 nm), and a GaAs upper cladding (30 nm).[67] The sample was then moved to a vacuum chamber, where it was kept at a constant temperature of 190 °C and exposed to a flux of hydrogen ions generated by a low energy Kaufman source (beam energy 100 eV, beam size about 3 cm) with an ion current density of 25 μA/cm^2 for about 500 s. The total dose of H was 8×10^{16} ions/cm^2, sufficient for a complete passivation of the nitrogen atoms. An excess of hydrogen has the only effect to favor the formation of N-2H-H complexes with respect to the N-2H ones, thus introducing a slightly compressive strain in the sample[33,45].

Membrane preparation. The sacrificial layer between the QW and the substrate was removed to obtain an array of well-separated circular suspended membranes with a diameter of few μm[32]. First, an array of circular apertures of 4 μm in diameter is patterned by Electron Beam Lithography (Vistec EPBG 5HR working at 100 kV) into a positive-tone resist (ZEP 520 A) spun on the sample's surface and developed in a mixture of MIBK:IPA (1:1). Then, the circular apertures are transfered into the sample, down to the AlGaAs layer, by means of a chlorine-based Reactive Ion Etching

(with a Cl_2:BCl_3:Ar gas mixture). Finally, the residual masking resist is removed with anisole, and the GaAs membranes are released by a wet etching in HF (5%) of the AlGaAs sacrificial layer.

QD fabrication. The QD fabrication was performed by exposing for a few seconds a nanometric region of the membrane surface, ideally the central region, with the 514.5 nm line of a continuous wave (CW) argon laser (Spectra-Physics BeamLok 2060) by means of a SNOM setup (Omicron TwinSNOM) in illumination mode, equipped with a dielectric tip. The laser shutter has a temporal reproducibility of about 10%. The tip is a chemically etched, uncoated near-field fiber probe, realized on a single mode optical fiber designed for operating at 633 nm[61,62]. The electromagnetic field at the exit of the tip is expected to maintain the cylindrical symmetry of the fiber. In order to guarantee this behavior, we have carefully selected the tips according to their far field projection on a target, selecting only the probes with a symmetrical far field distribution. The tip is mounted on a piezoelectric bimorph cantilever, controlled by feedback electronics to keep the tip at no more than 10 nm above the surface of the sample, which, in turn, is mounted on a three-axes piezo translation stage. The feedback signal can be recorded during the scanning of the sample surface, allowing to obtain, simultaneously with the optical map, also the topography of the scanned region, with a lateral spatial resolution below 50 nm. The tip was positioned on the center of each membrane at first by manual positioning, observing the sample surface with a microscope, and then it was repositioned after a topographic map of the surface. The width of the beam increases with the distance from the tip; in particular, considering the refractive index of our sample (3.5), the employed wavelength, and the characteristics of the fiber, the width of the beam in the layer of interest is expected to have a Gaussian shape with a FWHM of about (200 ± 50) nm, while the beam intensity can be considered constant along the vertical extension (6 nm) of the GaAsN:H layer[68].

PL characterization. The optical properties of the fabricated nanostructures were studied by micro-photoluminescence (micro-PL). The sample was kept at 10 K in a low-vibration Janis ST-500 continuous He-flow cryostat which in turn was mounted on a Physik Instrumente x-y translation stage for scanning the sample surface. The luminescence was collected by a home-made confocal microscope setup equipped with a infinity corrected Mitutoyo 100x objective (378-806-3, $\mathrm{NA} = 0.7$). The luminescence was spectrally dispersed and detected using an Acton SP2300i spectrograph mounting a 600 gr/mm grating, blazed at 1000 nm, and a Si CCD Acton Pixis 100F. The spatial resolution of the system is about 700 nm, while the spectral resolution is about 400 µeV. For time-integrated measurements the excitation source was a CW diode-pumped solid-state laser

at 532 nm (CNI MLL-III-532). Time-resolved PL (TR-PL) measurements were performed using the time correlated single photon counting (TCSPC) technique. The excitation source was provided by a mode-locked Ti:Sapphire tunable laser (Spectra Physics Tsunami, 700-900 nm spectral range, 200 fs pulse duration, 12.2 ns pulse period) frequency doubled by a BBO crystal and pumped by a frequency doubled CW Nd-YAG laser. The spectrally dispersed luminescence was selected using the exit slit of the spectrograph and sent to a PerkinElmer SPCM-AQR-16 single photon counting APD. For second-order autocorrelation ($g^{(2)}(\tau)$) measurements, a Hanbury Brown and Twiss intensity interferometer was used. The luminescence was split by a 50:50 non-polarizing beam splitter and each beam was dispersed by an Acton SP2300i spectrograph. A PerkinElmer SPCM-AQR-16 single photon counting APD was present at the exit slit of each spectrograph. Both for the TR-PL and $g^{(2)}(\tau)$ measurements the APD signals were processed with proper fast electronics (Tennelec TAC, Canberra MCA) interfaced with a computer.

SUPPORTING INFORMATION

Supporting Information is available from the Wiley Online Library or from the author.

ACKNOWLEDGMENTS

This work was supported by the Italian Ministry for Education, University and Research within the Futuro in Ricerca (FIRB) program (project DeLIGHTeD, Protocollo RBFR12RS1W). This work has also received funding from the European Union's Horizon 2020 research and innovation program under the Marie Sklodowska-Curie grant agreement No. 641899.

REFERENCES

[1] V. I. Klimov, ed., *Nanocrystal Quantum Dots* (CRC Press, 2010).

[2] K. D. Sattler, ed., *Handbook of Nanophysics: Nanoparticles and Quantum Dots* (CRC Press, 2011).

[3] M. A. Nielsen and I. L. Chuang, *Quantum Computation and Quantum Information* (Cambridge University Press, Cambridge, England, 2010).

[4] P. Michler, ed., *Single Semiconductor Quantum Dots* (Springer Berlin Heidelberg, 2009).

[5] P. Lodahl, S. Mahmoodian, and S. Stobbe, Rev. Mod. Phys. **87**, 347 (2015).

[6]J. Iles-Smith, D. P. S. McCutcheon, A. Nazir, and J. Mørk, Nat. Photonics **11**, 521 (2017).

[7]T. Grange, N. Somaschi, C. Antón, L. De Santis, G. Coppola, V. Giesz, A. Lemaître, I. Sagnes, A. Auffèves, and P. Senellart, Phys. Rev. Lett. **118**, 253602 (2017).

[8]D. Englund, D. Fattal, E. Waks, G. Solomon, B. Zhang, T. Nakaoka, Y. Arakawa, Y. Yamamoto, and J. Vučković, Phys. Rev. Lett. **95**, 013904 (2005).

[9]T. Yoshie, A. Scherer, J. Hendrickson, G. Khitrova, H. M. Gibbs, G. Rupper, C. Ell, O. B. Shchekin, and D. G. Deppe, Nature **432**, 200 (2004).

[10]D. Englund, A. Faraon, I. Fushman, N. Stoltz, P. Petroff, and J. Vučković, Nature **450**, 857 (2007).

[11]K. Hennessy, A. Badolato, M. Winger, D. Gerace, M. Atatüre, S. Gulde, S. Fält, E. L. Hu, and A. Imamoğlu, Nature **445**, 896 (2007).

[12]A. Hartmann, L. Loubies, F. Reinhardt, and E. Kapon, Appl. Phys. Lett. **71**, 1314 (1997).

[13]Y. Sugiyama, Y. Sakuma, S. Muto, and N. Yokoyama, Appl. Phys. Lett. **67**, 256 (1995).

[14]A. Mohan, P. Gallo, M. Felici, B. Dwir, A. Rudra, J. Faist, and E. Kapon, Small **6**, 1268 (2010).

[15]P. Gallo, M. Felici, B. Dwir, K. A. Atlasov, K. F. Karlsson, A. Rudra, A. Mohan, G. Biasiol, L. Sorba, and E. Kapon, Appl. Phys. Lett. **92**, 263101 (2008).

[16]B. Rigal, C. Jarlov, P. Gallo, B. Dwir, A. Rudra, M. Calic, and E. Kapon, Appl. Phys. Lett. **107**, 141103 (2015).

[17]A. Lyasota, C. Jarlov, P. Gallo, A. Rudra, B. Dwir, and E. Kapon, Appl. Phys. Lett. **111**, 053103 (2017).

[18]M. Calic, C. Jarlov, P. Gallo, B. Dwir, A. Rudra, and E. Kapon, Sci. Rep. **7**, 4100 (2017).

[19]L. O. Mereni, V. Dimastrodonato, R. J. Young, and E. Pelucchi, Appl. Phys. Lett. **94**, 223121 (2009).

[20]P. J. Poole, D. Dalacu, J. Lefebvre, and R. L. Williams, Nanotechnology **21**, 295302 (2010).

[21]D. Chithrani, R. L. Williams, J. Lefebvre, P. J. Poole, and G. C. Aers, Appl. Phys. Lett. **84**, 978 (2004).

[22]D. Dalacu, K. Mnaymneh, V. Sazonova, P. J. Poole, G. C. Aers, J. Lapointe, R. Cheriton, A. J. SpringThorpe, and R. Williams, Phys. Rev. B **82**, 033301 (2010).

[23]S. Jeppesen, M. S. Miller, B. Kowalski, I. Maximov, and L. Samuelson, Superlattices Microstruct. **23**, 1347 (1998).

[24]P. Atkinson, M. B. Ward, S. P. Bremner, D. Anderson, T. Farrow, G. A. C. Jones, A. J. Shields, and D. A. Ritchie, Jpn. J. Appl. Phys. **45**, 2519 (2006).

[25]K. D. Jöns, P. Atkinson, M. Müller, M. Heldmaier, S. M. Ulrich, O. G. Schmidt, and P. Michler, Nano Lett. **13**, 126 (2013).

[26]A. Jamil, J. Skiba-Szymanska, S. Kalliakos, A. Schwagmann, M. B. Ward, Y. Brody, D. J. P. Ellis, I. Farrer, J. P. Griffiths, G. A. C. Jones, D. A. Ritchie, and A. J. Shields, Appl. Phys. Lett. **104**, 101108 (2014).

[27]S. Kohmoto, H. Nakamura, T. Ishikawa, and K. Asakawa, Appl. Phys. Lett. **75**, 3488 (1999).

[28]M. Kitamura, M. Nishioka, J. Oshinowo, and Y. Arakawa, Appl. Phys. Lett. **66**, 3663 (1995).

[29]H. Lee, J. A. Johnson, J. S. Speck, and P. M. Petroff, J. Vac. Sci. Technol. B **18**, 2193 (2000).

[30]S. Kalliakos, C. P. García, V. Pellegrini, M. Zamfirescu, L. Cavigli, M. Gurioli, A. Vinattieri, A. Pinczuk, B. S. Dennis, L. N. Pfeiffer, and K. W. West, Appl. Phys. Lett. **90**, 181902 (2007).

[31]S. Birindelli, M. Felici, J. S. Wildmann, A. Polimeni, M. Capizzi, A. Gerardino, S. Rubini, F. Martelli, A. Rastelli, and R. Trotta, Nano Lett. **14**, 1275 (2014).

[32]G. Pettinari, A. Gerardino, L. Businaro, A. Polimeni, M. Capizzi, M. Hopkinson, S. Rubini, F. Biccari, F. Intonti, A. Vinattieri, M. Gurioli, and M. Felici, Microelectron. Eng. **174**, 16 (2017).

[33]G. Ciatto, ed., *Hydrogenated Dilute Nitride Semiconductors* (Pan Stanford Publishing, 2015).

[34]A. Erol, ed., *Dilute III-V Nitride Semiconductors and Material Systems* (Springer, 2008).

[35]D. B. Jackrel, S. R. Bank, H. B. Yuen, M. A. Wistey, J. S. Harris, A. J. Ptak, S. W. Johnston, D. J. Friedman, and S. R. Kurtz, J. Appl. Phys. **101**, 114916 (2007).

[36]M. Henini, ed., *Dilute Nitride Semiconductors* (Elsevier, 2005).

[37]M. Baranowski and J. Misiewicz, J. Appl. Phys. **118**, 155705 (2015).

[38]E. P. O'Reilly, A. Lindsay, P. J. Klar, A. Polimeni, and M. Capizzi, Semicond. Sci. Technol. **24**, 033001 (2009).

[39]M. Morifuji and F. Ishikawa, Physica B **485**, 89 (2016).

[40]G. Pettinari, F. Masia, A. Polimeni, M. Felici, A. Frova, M. Capizzi, A. Lindsay, E. P. O'Reilly, P. J. Klar, W. Stolz, G. Bais, M. Piccin, S. Rubini, F. Martelli, and A. Franciosi, Phys. Rev. B **74**, 245202 (2006).

[41]J. Plaza, J. L. Castaño, B. J. García, H. Carrère, and E. Bedel-Pereira, Appl. Phys. Lett. **86**, 121918 (2005).

[42]K. Uesugi, I. Suemune, T. Hasegawa, T. Akutagawa, and T. Nakamura, Appl. Phys. Lett. **76**, 1285 (2000).

[43]F. Jiang, M. Stavola, M. Capizzi, A. Polimeni, A. A. Bonapasta, and F. Filippone, Phys. Rev. B **69**, 041309(R) (2004).

[44]L. Wen, F. Bekisli, M. Stavola, W. B. Fowler, R. Trotta, A. Polimeni, M. Capizzi, S. Rubini, and F. Martelli, Phys. Rev. B **81**, 233201 (2010).

[45]L. Wen, M. Stavola, W. B. Fowler, R. Trotta, A. Polimeni, M. Capizzi, G. Bisognin, M. Berti, S. Rubini, and F. Martelli, Phys. Rev. B **86**, 085206 (2012).

[46]P. J. Klar, H. Grüning, M. Güngerich, W. Heimbrodt, J. Koch, T. Torunski, W. Stolz, A. Polimeni, and M. Capizzi, Phys. Rev. B **67**, 121206(R) (2003).

[47]A. Polimeni, G. B. H. v., H. M. Bissiri, M. Capizzi, M. Fischer, M. Reinhardt, and A. Forchel, Phys. Rev. B **63**, 201304(R) (2001).

[48]A. Polimeni, M. Bissiri, M. Felici, M. Capizzi, I. A. Buyanova, W. M. Chen, H. P. Xin, and C. W. Tu, Phys. Rev. B **67**, 201303(R) (2003).

[49]F. Masia, G. Pettinari, A. Polimeni, M. Felici, A. Miriametro, M. Capizzi, A. Lindsay, S. B. Healy, E. P. O'Reilly, A. Cristofoli, G. Bais, M. Piccin, S. Rubini, F. Martelli, A. Franciosi, P. J. Klar, K. Volz, and W. Stolz, Phys. Rev. B **73**, 073201 (2006).

[50]M. Geddo, E. Giulotto, M. S. Grandi, M. Patrini, R. Trotta, A. Polimeni, M. Capizzi, F. Martelli, and S. Rubini, Appl. Phys. Lett. **101**, 191908 (2012).

[51]M. Berti, G. Bisognin, D. D. Salvador, E. Napolitani, S. Vangelista, A. Polimeni, M. Capizzi, F. Boscherini, G. Ciatto, S. Rubini, F. Martelli, and A. Franciosi, Phys. Rev. B **76**, 205323 (2007).

[52]M. Felici, R. Trotta, F. Masia, A. Polimeni, A. Miriametro, M. Capizzi, P. J. Klar, and W. Stolz, Phys. Rev. B **74**, 085203 (2006).

[53]M. Felici, A. Polimeni, G. Salviati, L. Lazzarini, N. Armani, F. Masia, M. Capizzi, F. Martelli, M. Lazzarino, G. Bais, M. Piccin, S. Rubini, and A. Franciosi, Adv. Mater. **18**, 1993 (2006).

[54]R. Trotta, A. Polimeni, M. Capizzi, F. Martelli, S. Rubini, M. Francardi, A. Gerardino, and L. Mariucci, Appl. Phys. Lett. **94**, 261905 (2009).

[55]R. Trotta, A. Polimeni, F. Martelli, G. Pettinari, M. Capizzi, L. Felisari, S. Rubini, M. Francardi, A. Gerardino, P. C. M. Christianen, and J. C. Maan, Adv. Mater. **23**, 2706 (2011).

[56]R. Trotta, L. Cavigli, L. Felisari, A. Polimeni, A. Vinattieri, M. Gurioli, M. Capizzi, F. Martelli, S. Rubini, L. Mariucci, M. Francardi, and A. Gerardino, Phys. Rev. B **81**, 235327 (2010).

[57]M. Felici, G. Pettinari, F. Biccari, A. Boschetti, S. Birindelli, S. Younis, M. Gurioli, A. Vinattieri, A. Gerardino, L. Businaro, M. Hopkinson, S. Rubini, M. Capizzi, and A. Polimeni, Phys. Rev. X (2017), under review.

[58]N. Balakrishnan, A. Patanè, O. Makarovsky, A. Polimeni, M. Capizzi, F. Martelli, and S. Rubini, Appl. Phys. Lett. **99**, 021105 (2011).

[59]N. Balakrishnan, G. Pettinari, O. Makarovsky, L. Turyanska, M. W. Fay, M. D. Luca, A. Polimeni, M. Capizzi, F. Martelli, S. Rubini, and A. Patanè, Phys. Rev. B **86**, 155307 (2012).

[60]A. Zayats and D. Richards, eds., *Nano-Optics and Near-Field Optical Microscopy* (Artech House, 2009).

[61]P. Lambelet, A. Sayah, M. Pfeffer, C. Philipona, and F. Marquis-Weible, Appl. Opt. **37**, 7289 (1998).

[62]R. Stöckle, C. Fokas, V. Deckert, R. Zenobi, B. Sick, B. Hecht, and U. P. Wild, Appl. Phys. Lett. **75**, 160 (1999).

[63]M. Abbarchi, C. Mastrandrea, T. Kuroda, T. Mano, A. Vinattieri, K. Sakoda, and M. Gurioli, J. Appl. Phys. **106**, 053504 (2009).

[64]N. Dotti, F. Sarti, S. Bietti, A. Azarov, A. Kuznetsov, F. Biccari, A. Vinattieri, S. Sanguinetti, M. Abbarchi, and M. Gurioli, Phys. Rev. B **91**, 205316 (2015).

[65]M. Abbarchi, T. Kuroda, T. Mano, K. Sakoda, C. A. Mastrandrea, A. Vinattieri, M. Gurioli, and T. Tsuchiya, Phys. Rev. B **82**, 201301(R) (2010).

[66]H. C. Casey, D. D. Sell, and K. W. Wecht, J. Appl. Phys. **46**, 250 (1975).

[67]J. M. Ulloa, P. M. Koenraad, and M. Hopkinson, Appl. Phys. Lett. **93**, 083103 (2008).

[68]F. Intonti, *Near-field optical spectroscopy of disorder in semiconductor nanostructures*, Ph.D. thesis, Humboldt-Universität Berlin (2002), published by Mensch & Buch. ISBN 978-3898204156.